

Effects of rotation on the Lyman- α line morphology in distant galaxies

Nicolas Garavito-Camargo.¹ Jaime E. Forero-Romero²

¹ *Uni A* ² *Uni B*

22 February 2013

ABSTRACT

Key words: galaxies: high-redshift - galaxies: star formation - line: formation

1 INTRODUCTION

Due to the resonant nature of the Lyman α line, gas kinematics play an important role shaping its morphology. In the literature there has been extensive studies of outflow/inflow configurations.

In this paper we study for the first time the impact of rotation on the morphology of the Lyman α line. To isolate the effects of rotation we focus on a simple system: the gas distribution is spherical, with homogenous density and the gas rotates as a solid body.

This paper is structured as follows.

2 IMPLEMENTATION OF BULK GAS ROTATION

We implement into CLARA the simplest model whereby a sphere rotates with homogeneous angular velocity. We define a cartesian coordinate system with its origin at the center of the sphere and the rotation axis to be the z -axis, the components in the bulk velocity field, $\vec{v} = v_x \hat{i} + v_y \hat{j} + v_z \hat{k}$, in the gas can be written as

$$v_x = -\frac{y}{R} V_{\max}, \quad (1a)$$

$$v_y = \frac{x}{R} V_{\max}, \quad (1b)$$

$$v_z = 0, \quad (1c)$$

where R is the radius of the sphere and V_{\max} is the linear velocity at the sphere's surface. The minus sign in the x -component of the velocity indicates the direction of rotation, in this case we assume that the angular velocity vector goes in the \hat{k} direction. The linear dependence of the velocity on the radial distance describes the case of constant angular velocity $\omega = V_{\max}/R$.

We take the polar angle θ that a unitary vector makes with the rotation axis as defined by the dot product $\cos \theta = \hat{u} \cdot \hat{k}$. In the Section 4 we will present in detail how the line differs at different observing angles θ .

Velocity (km s ⁻¹)	V_{\max}	0, 50, 100, 200, 300
Hydrogen Optical Depth	τ_H	10 ⁵ , 10 ⁶ , 10 ⁷
Dust Optical Depth	τ_A	XXX
Photons Distributions		Central, Homogeneous

Table 1. Values for the varying input parameters in CLARA. Taking into account all the possible combinations for these models

3 GRID OF SIMULATED MODELS

We compute the emergent Lyman- α line for several models with different values for the maximal rotational velocity, hydrogen optical depth, dust optical depth and initial distributions of the photons with respect to the gas. There are in total 60 models with the input parameters summarized in Table 1.

4 RESULTS

The central result of this paper is summarized in Figure 4 where we show that rotation has a considerable effect on the morphology of the emergent Lyman- α line both in the case where the photons are emitted at the sphere's center and when they are initialized with an homogeneous distribution all over the gas volume.

The results for this outgoing spectra are integrated over the whole sphere, meaning that all the escaping photons were taken into account regardless of the direction of the outgoing photons. Figure ?? shows how if one gives a weight to each outgoing photon according to its direction when escaping the gas distribution it is possible to detect notable differences in the spectrum for different viewing angles.

4.1 Maxima Positions

The maximum position gives information about the wavelength of the majority of the outgoing photons after they interact with the gas, in addition as a photon has more

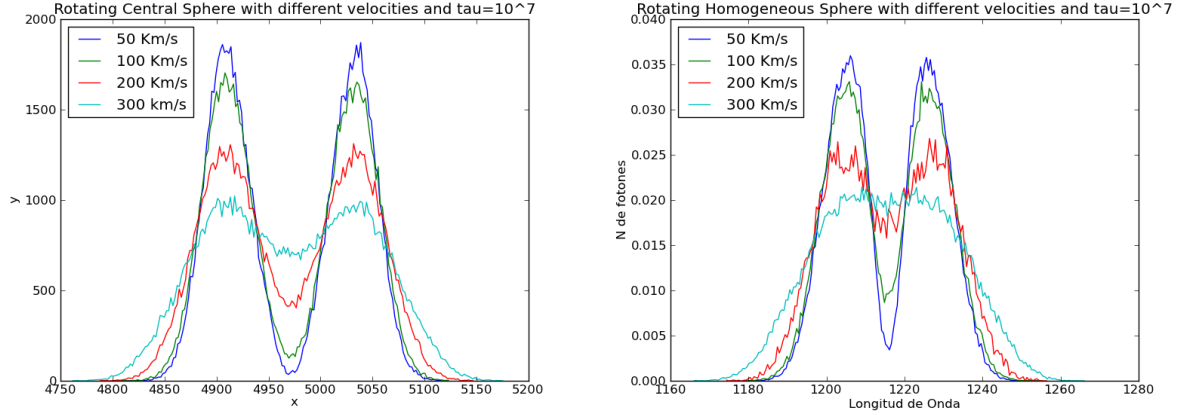


Figure 1. Shape of the Lyman alpha line for different velocities. The left (right) panel shows the central (homogeneous) photon distribution.

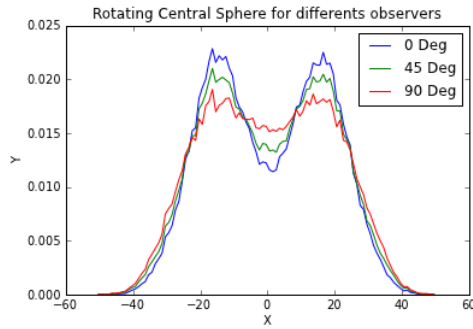


Figure 2. Spectra for different observers. Model: $V = 300 \text{ km s}^{-1}$, Optical Depth $\tau = 10^7$ and Central Distribution without dust.

scatterings its wave length would be larger than the initial which is 1216 \AA . As we can see in Figure 4.1 the position of the maxima does not change with rotational velocity for the central distribution. On the other hand for the homogeneous distribution the maxima position X_m change for $\text{Log}_{10}\tau = 5$, this is because at higher rotational velocities photons escape with less scatterings, for $v = 100 \text{ km s}^{-1}$ the majority of the photons still escape with scatterings but for $v = 200 \text{ km s}^{-1}$ the number of photons that escape with a few or any scatterings is higher, this is why the maxima change to the center of the spectra.

If we now study the effect of the optical depth τ in the maxima position X_m Figure 4.1, we found that as the optical depth increase (include reference of previous articles) the maxima position increase and this is a well known result, but when rotation is included the dependence is not linear.

4.2 Line Equivalent Width

The width of the line provide information of how many photons escape with a particular wave length, in the ideal case in which all the photons escape with the same wave length the outgoing spectrum would be narrower. We found a dependency of the equivalent width with the

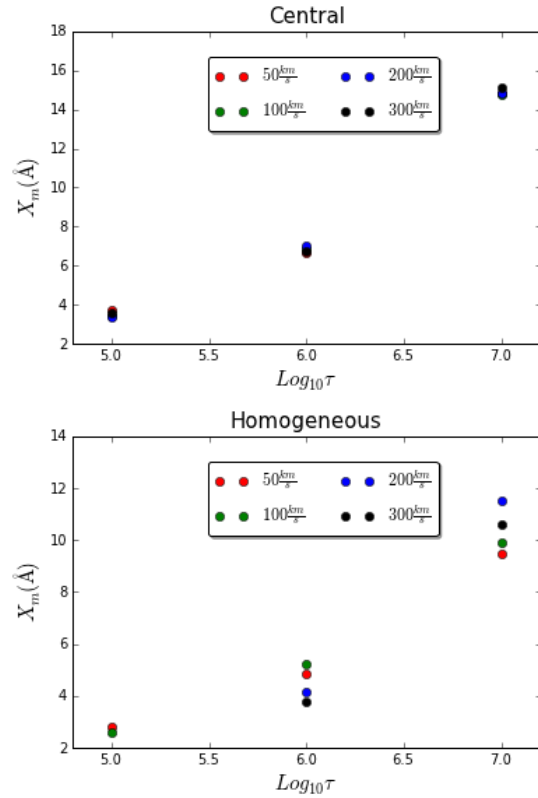


Figure 3. Position of the maxima in the outgoing spectra for different Optical Depths, (up) Central Distribution, (Down) Homogeneous Distribution.

rotation of the gas cloud for all the models we study, this is shown in Figure 4.2. As velocity increase also the equivalent width increase, it means that some photons escape with fewer scatterings than the static case but at the same time some photons escape with more scatterings.

We also found that the equivalent width is not the same for different angles of observation in particular as the angle increase the width also increase Figure ??, this is related

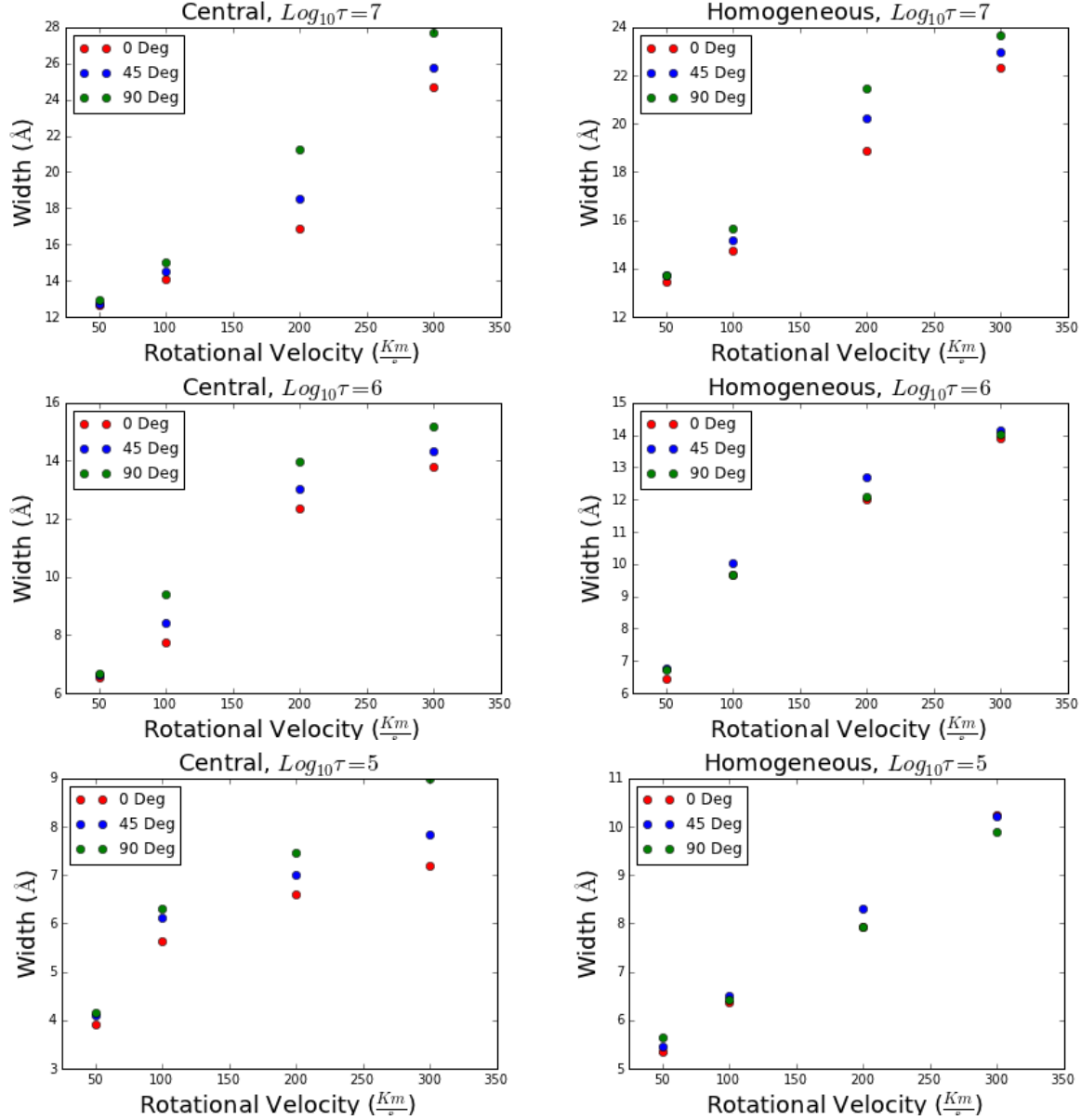


Figure 5. Width of the lyman-alpha line for all the models.

with the fact that photons escape easily (with less scatterings) in the \hat{k} direction

Following the convention of Verhamme et al 2012 we define $\mu = \cos(\theta)$, we can make a polynomial fit the $EW(\mu)$ for our models, this is resumed in Table 2

4.3 Escape Fraction

The fraction of photons that escape from the cloud of gas and dust is defined as:

$$F_e = \frac{\sum_{NI} \vec{k} \cdot \vec{\sigma}}{\sum_{NF} \vec{k} \cdot \vec{\sigma}} \quad (2)$$

Where NI is the initial number of photons and NF is the final. This escape fraction is computed for all the

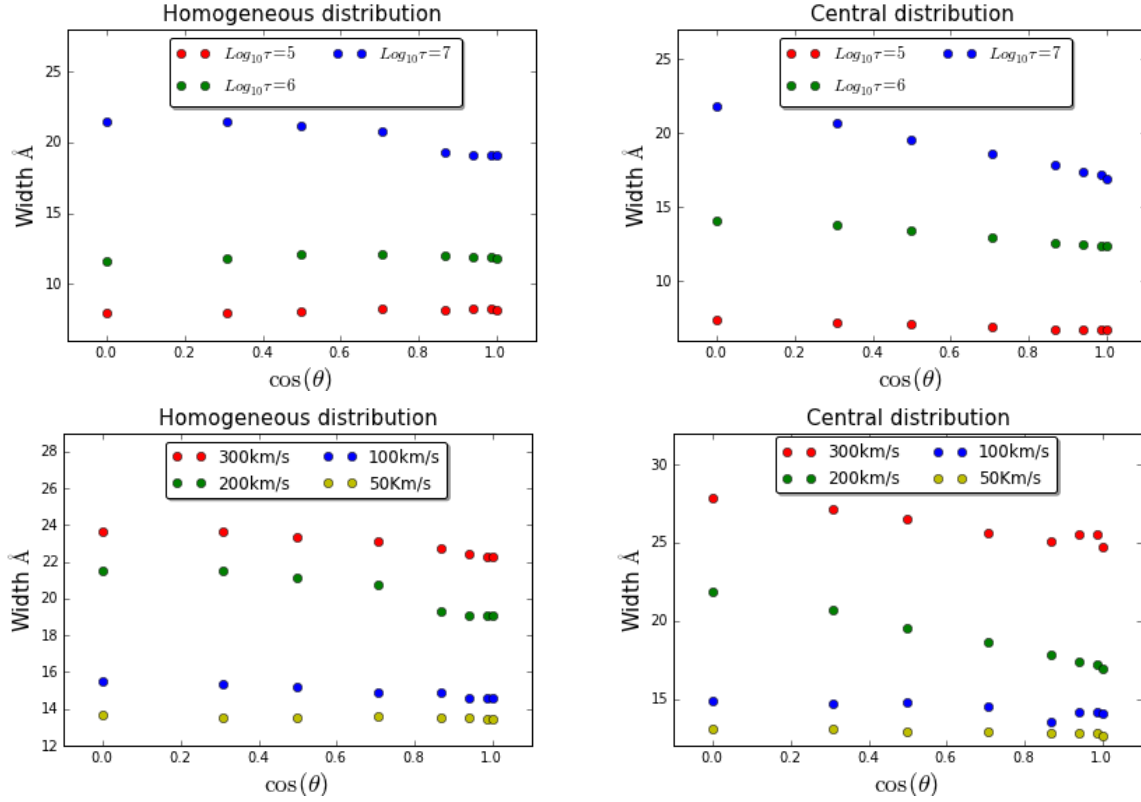
models which results are shown in Fig.[6]

When the distribution is homogeneous the effect of velocity in the escape fraction is clear while in the central model the effect is not notorious. The main effect is that the escape fraction increase as the velocity increase.

5 DISCUSSION

6 OBSERVATIONAL IMPLICATIONS

... The results derived in this paper have consequences on the interpretation of galaxy observations in the Lyman alpha line.

**Figure 6.** Width of the lyman-alpha line for all the models.

Model	Fit
Central, $\tau = 10^5$, $V = 200 \text{ km s}^{-1}$	$EW(\mu) = -59 - 1677\mu - 17864\mu^2 + 84509\mu^3 - 149877\mu^4$
Central, $\tau = 10^6$, $V = 200 \text{ km s}^{-1}$	$EW(\mu) = -1 + 53.8\mu - 1080\mu^2 + 9644\mu^3 - 32264\mu^4$
Central, $\tau = 10^7$, $V = 200 \text{ km s}^{-1}$	$EW(\mu) = 0.011 + 0.9\mu - 27\mu^2 + 359\mu^3 - 1791\mu^4$
Hom, $\tau = 10^5$, $V = 200 \text{ km s}^{-1}$	$EW(\mu) = 11.66 - 187.22\mu - 54.58\mu^2 + 12932.5\mu^3 - 51882.9\mu^4$
Hom, $\tau = 10^6$, $V = 200 \text{ km s}^{-1}$	$EW(\mu) = -361.64 + 17158.92\mu - 305268.4\mu^2 + 2413478\mu^3 - 7154649\mu^4$
Hom, $\tau = 10^7$, $V = 200 \text{ km s}^{-1}$	$EW(\mu) = -0.28 + 23.29\mu - 721\mu^2 + 9912\mu^3 - 51074\mu^4$

Table 2. Fits for EW models

Velocity (Km/s)	Maximum 1 position	Maximum 2 position
50	-16.2695	16.23705
100	-15.66496	15.33504
200	-16.93149	14.56851
300	-13.40048	16.09952

Table 3. Optical Depth $\tau = 10^7$, Central Distribution

7 CONCLUSIONS

ACKNOWLEDGEMENTS

APPENDIX A: TABLES

Line width

Escape fraction

Velocity (km/s)	Maximum 1 position	Maximum 2 position
50	-7.46286	6.53714
100	-7.53357	6.96643
200	-8.17453	7.32547
300	-6.81487	6.18513

Table 4. Optical Depth $\tau = 10^6$, Central Distribution

Velocity(Km/s)	Maximum 1 position	Maximum 2 position
50	-4.33708	3.66292
100	-4.27326	3.72674
200	-3.7737	3.7263
300	-3.84903	4.15097

Table 5. Optical Depth $\tau = 10^5$, Central distribution

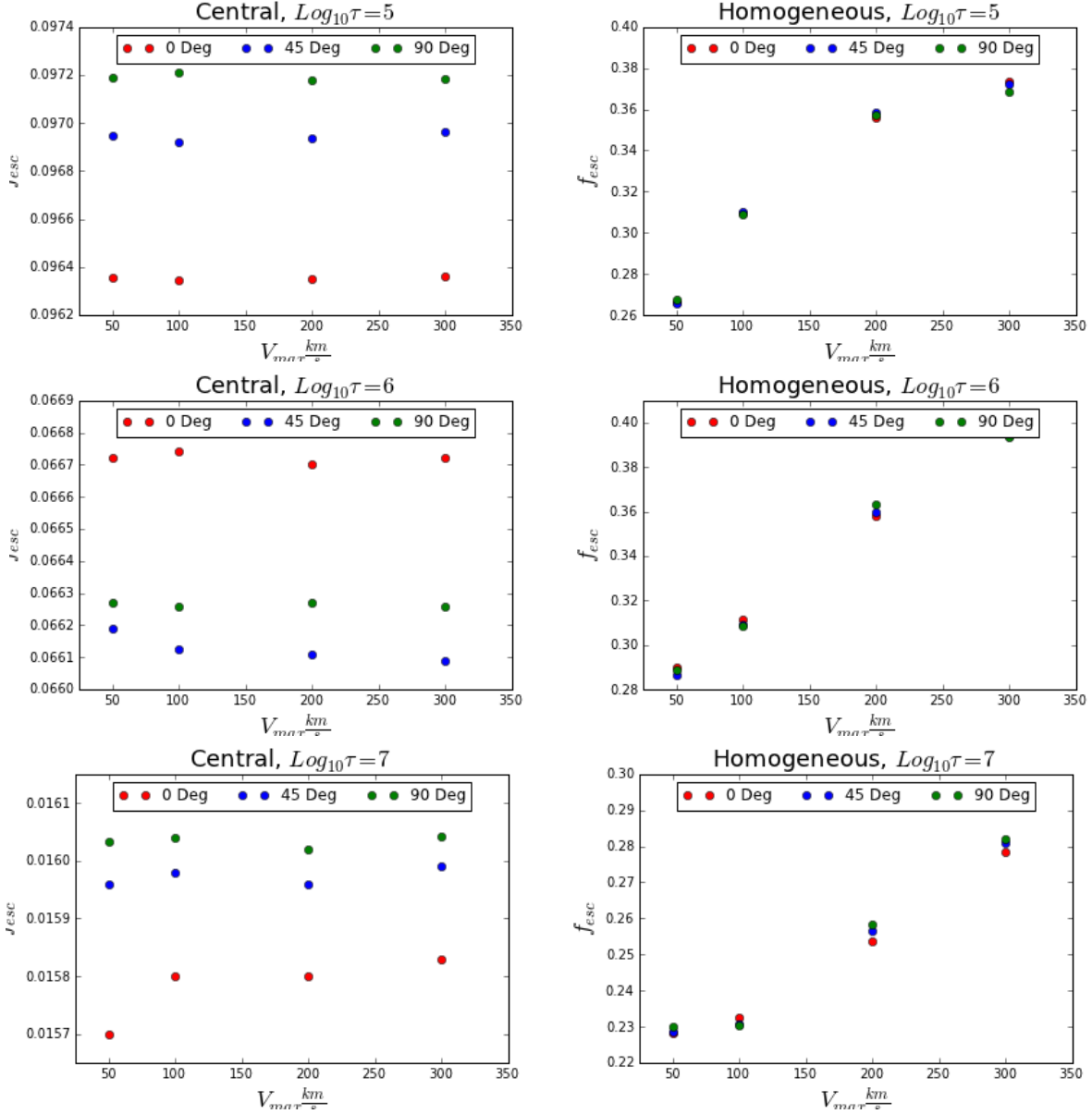


Figure 7. Escape fraction for all the models. Left panels show the central distribution, while right panels show the homogeneous distribution

Velocity(Km/s)	FWHM	θ
50	12.62	0°
50	12.72	45°
50	12.93	90°
100	14.07	0°
100	14.48	45°
100	15.00	90°
200	16.90	0°
200	18.51	45°
200	21.24	90°
300	24.69*	0°
300	25.79*	45°
300	27.73*	90°

Table 6. Lines Widths for a Central Distribution and $\tau = 10^7$

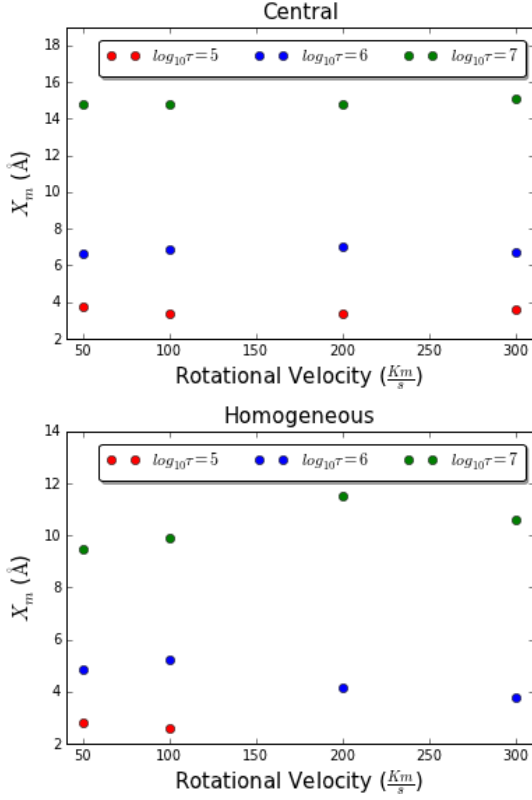


Figure 4. Position of the maxima in the outgoing spectra for different Rotational velocities, (up) Central Distribution, (Down) Homogeneous Distribution.

[H]

Model	Velocity (km/s)	θ	Dust $\Sigma(s)$	$\Sigma(s)$
Homogeneous	50	0°	13293.06	49939.53
Homogeneous	50	45°	13291.04	50001.59
Homogeneous	50	90°	13348.76	49922.73
Homogeneous	100	0°	15527.69	50114.11
Homogeneous	100	45°	15511.56	49967.17
Homogeneous	100	90°	15401.71	49833.65
Homogeneous	200	0°	17830.85	50078.69
Homogeneous	200	45°	17932.87	50064.42
Homogeneous	200	90°	17830.85	49931.748
Homogeneous	300	0°	18687.33	50048.33
Homogeneous	300	45°	18572.12	49922.67
Homogeneous	300	90°	18421.79	49979.37

Table 7. Escape fraction for a Homogeneous Distribution and optical depth 10^5 .

Model	Velocity (km/s)	θ	Dust $\Sigma(s)$	$\Sigma(s)$
Central	50	0°	4809.881	49917.069
Central	50	45°	4829.21	49811.79
Central	50	90°	4845.108	49853.039
Central	100	0°	4809.665	49921.30
Central	100	45°	4828.65	49820.13
Central	100	90°	4846.45	49854.0
Central	200	0°	4809.63	49917.64
Central	200	45°	4829.25	49818.49
Central	200	90°	4844.89	49856.66
Central	300	0°	4810.56	49922.98
Central	300	45°	4831.16	49823.33
Central	300	90°	4845.33	49858.48

Table 8. Escape fraction for the central Distribution and optical depth 10^5 .